$^3\mathrm{H}(\vec{p},\gamma)^4\mathrm{He}$ reaction below $E_p = 80$ keV

R. S. Canon, S. O. Nelson, K. Sabourov, E. Wulf, and H. R. Weller
Department of Physics, Duke University, Durham, North Carolina 27708
and Triangle Universities Nuclear Laboratory, Durham, North Carolina 27708

R. M. Prior and M. Spraker
Department of Physics, North Georgia College and State University, Dahlonega, Georgia 30597
and Triangle Universities Nuclear Laboratory, Durham, North Carolina 27708

J. H. Kelley and D. R. Tilley
Department of Physics, North Carolina State University, Raleigh, North Carolina 27696
and Triangle Universities Nuclear Laboratory, Durham, North Carolina 27708

(Received 23 April 2001; published 4 April 2002)

The $^3\mathrm{H}(\vec{p},\gamma)^4\mathrm{He}$ reaction was studied at incident energies of $E_p = 40$ and 80 keV at the Triangle Universities Nuclear Laboratory (TUNL) using beams from a polarized ion source. The present study was the logical progression of a previous study of the $^2\mathrm{H}(\vec{p},\gamma)^3\mathrm{He}$ reaction done by the radiative capture group at TUNL. The angular distributions of the cross section, $\sigma(\theta)$, and the analyzing power, $A_y(\theta)$, were measured at incident proton beam energies of 40 keV and 80 keV. In both cases the beam was stopped in the target. The magnetic dipole transition strength was determined from the results of a TME analysis. A comparison of the $M1$ strength with that seen in similar reactions in the three-nucleon case made it possible to infer the meson-exchange current origin of most of this strength. Previous measurements of the absolute cross section extended down to beam energies of 100 keV. The present study extends the measured cross section data to lower energies and is consistent with the previous results. A parametrization of the astrophysical S factor including both data sets was performed.

DOI: 10.1103/PhysRevC.65.044008 PACS number(s): 21.45.+v, 24.70.+s, 25.10.+s, 25.40.Lw

I. INTRODUCTION

Previous polarized proton and deuteron capture studies at very low energies (~ 80 keV) have revealed the sensitivity of polarization observables to explicit meson-exchange current (MEC) effects in the case of the three-body system ^{3}He [1,2]. It was found, for example, that the measured values of the vector analyzing power A_y for the $d(p,\gamma)^3$He reaction differed by a factor of 2 from theory unless explicit MEC effects were taken into account. This can be understood as arising from the $M1$ strength which is substantial at these low energies since it is the result of s-wave capture. The situation is similar to the situation in the case of n-d capture at thermal energies. This process is known to be entirely due to s-wave capture, entirely $M1$ radiation, and has a measured cross section which differs by a factor of 2 from the theoretically calculated cross section without the inclusion of two-body currents, i.e., MEC effects [3]. The relatively large MEC effects present in this $M1$ strength have been known for some time to be the result of the suppression of the one-body transition strength which arises from the quasiorthogonality of the continuum and the ground states [4,5].

Similar studies are now being undertaken in the case of the four-nucleon system ^{4}He. This paper will report the results of measurements of the $^3\mathrm{H}(\vec{p},\gamma)^4\mathrm{He}$ reaction at $E_p = 40$ and 80 keV. The effects which lead to a strong MEC contribution in the $n+d$ thermal neutron capture cross section are expected to be even stronger in the four-body system. In the case of thermal neutron capture on ^{3}He, for example, the calculated cross section was found to be almost entirely due to exchange currents [6]. Following along the lines of our previous studies using the $\vec{p}+d$ and the $\vec{d}+p$ capture reactions, we have also made measurements of the analyzing power in the $\vec{p}+{}^3\mathrm{H}$ capture reaction at and below $E_p = 80$ keV. This analyzing power, especially at 90°, should be very sensitive to the presence of $M1$ strength (through its interference with the dominant $E1$ strength) and, in turn, very sensitive to the presence of explicit MEC effects in the four-body system.

Unfortunately, unlike the $A=3$ system, where *ab initio* calculations which include two-body current effects exist [7], there are presently no $A=4$ calculations of a similar nature. It is hoped that the present work will encourage such calculations, which are reportedly presently underway [8,9]. Nevertheless, we will perform a direct comparison of the ratio of the $M1$ effects in the p-d and the n-d capture reactions to the same ratio found in the p-^{3}H and n-^{3}He capture reactions in this low-energy regime. The result can be interpreted to mean that the $M1$ strength which is deduced from our measured analyzing powers is consistent with that observed in the case of thermal neutron capture on ^{3}He when the effects of the Coulomb barrier are taken into account. This result implies that the $M1$ strength in the p-^{3}H capture reaction and, therefore, the observed analyzing powers at these energies arise almost entirely as a result of explicit MEC effects in the four-body system. The present data are also used to determine the cross section and the astrophysical S factor below 100 keV. The results are found to be consistent with

previous results at and above 100 keV [6]. The present results are combined with the previous data in order to perform an extrapolation to near-zero energies.

II. EXPERIMENTAL DETAILS

This experiment was performed using 80 keV and 40 keV polarized proton beams directly out of the TUNL Atomic Beam Polarized Ion Source (ABPIS) [10]. The Spin-Filter polarimeter [11] was used to measure the beam polarization, which was typically 0.65 ± 0.02. The spin-up and spin-down polarized beams were switched at the rate of 10 Hz. Since the beam is in an indeterminate state of polarization during a switch, data taking was stopped for 7 ms while this occurred. Typical beam currents on target were limited to about 10 μA in order to minimize target deterioration.

The targets used in this work were tritiated titanium foils [12], and the beam was stopped in the target. These targets contained about 0.5 tritium atoms for every titanium atom. (The targets were manufactured in 1990, so that 40% of their original tritium content had decayed.) The tritium density was measured by means of the ^{3}H$(d,n)^4$He reaction [13], at incident beam energies of 40, 60, and 80 keV—all of which were stopped in the target. The outgoing alpha particles were detected at back angles using a silicon-surface-barrier detector. The tritium density was determined from the measured yields using the known cross sections [13] and stopping powers [14], performing the convolution integral, and then solving for the tritium volume density. Our data also implied a decrease in the tritium density as the beam energy was lowered, indicating a variation in the tritium density as a function of depth in the target. This made it necessary to model the tritium profile. Various profiles were assumed including a fully depleted surface region followed by a partially depleted zone, a fully depleted region followed by a gradient region of arbitrary slope, a uniformly partially depleted target, and an exponential form with and without a depleted surface region. The best fit to the yields of the ^{3}H$(d,n)^4$He reaction was obtained by assuming a fully depleted region of 0.15 μm thickness followed by a region loaded to 0.46 tritium nuclei for each titanium nucleus ($\chi^2/\nu = 1.4$). Finally, we note that contaminant ^{4}He particles from any residual ^{3}He in the target can be ignored since the cross section for the ^{3}He$(d,p)^4$He reaction [15] is over 100 times less than that for the ^{3}H$(d,n)^4$He reaction [13].

The targets were cooled by means of a liquid nitrogen cold finger. This was found to be essential in order to preserve the tritium content. Further cold traps and baffles were used to make sure that no contaminants were deposited on the target surface and to contain any tritium which escaped from the targets. Visual examination of the target surface condition as well as careful monitoring of the counting rate as a function of time were used to verify the absence of surface contamination and/or target deterioration. Possible tritium losses were monitored in two ways. First, tritium monitors were installed on the exit ports of all mechanical backing and roughing pumps on the beamline and target chamber. A low threshold (10 μC/m^3) assured us that losses were negligibly small. In addition to this, periodic wipe tests were performed on parts of the chamber and beamline in the vicinity of the target, especially those which were cold surfaces intended to trap any escaping tritium. Measurements here never exceeded several μC/cm^2, indicating negligible losses.

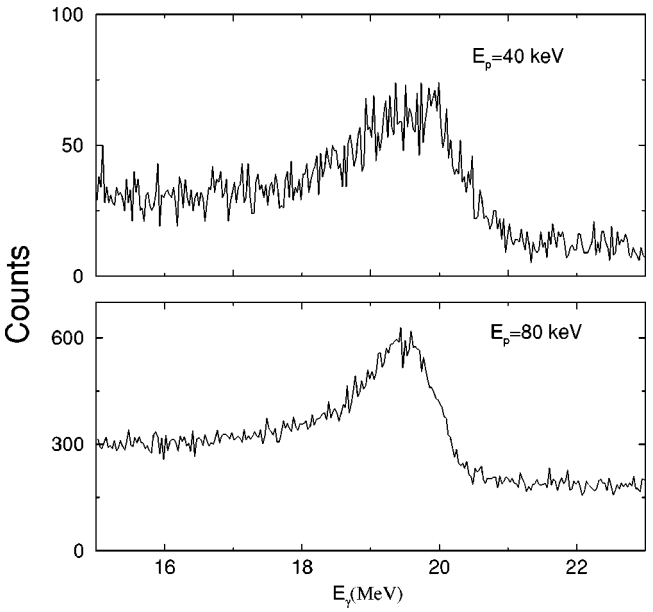

FIG. 1. The spectra obtained at $E_p = 40$ and 80 keV using a 10 in.$\times$10 in. NaI detector. The 40 keV spectrum was obtained using, in addition, a plastic scintillator anticoincidence shield. The background due to cosmic rays was subtracted from the spectra before obtaining the final yields.

The 19.8 MeV γ rays were detected in 10 in.$\times$10 in. NaI detectors, whose energy response functions and efficiencies were well known [16]. As a result of the high energy of the outgoing γ rays, the only background in the peak region was that due to cosmic rays. While this was not a problem in the 80 keV case, the low counting rate of true events at 40 keV required the use of a plastic anticoincidence shield, which was able to reject about 98% of the cosmic-ray background. Typical spectra at 80 and at 40 keV are shown in Fig. 1. As can been seen in this figure, the background to foreground ratio in the 80 keV data was much less than that in the 40 keV case as a result of the much lower counting rate at 40 keV, despite the use of the active shield at 40 keV. These backgrounds, which arise almost entirely from cosmic-ray-induced events, were subtracted from the data before the peaks were summed. The summing region was established by fitting the data to our previously determined [17] detector response function, obtaining a width and centroid, and then summing from two widths below to one width above the centroid.

III. RESULTS

Angular distributions of the cross section and the analyzing power were obtained at incident proton beam energies of 40 and 80 keV, both beams being stopped in the target. The data are shown in Fig. 2.

Only *s*-wave and *p*-wave capture are expected to be

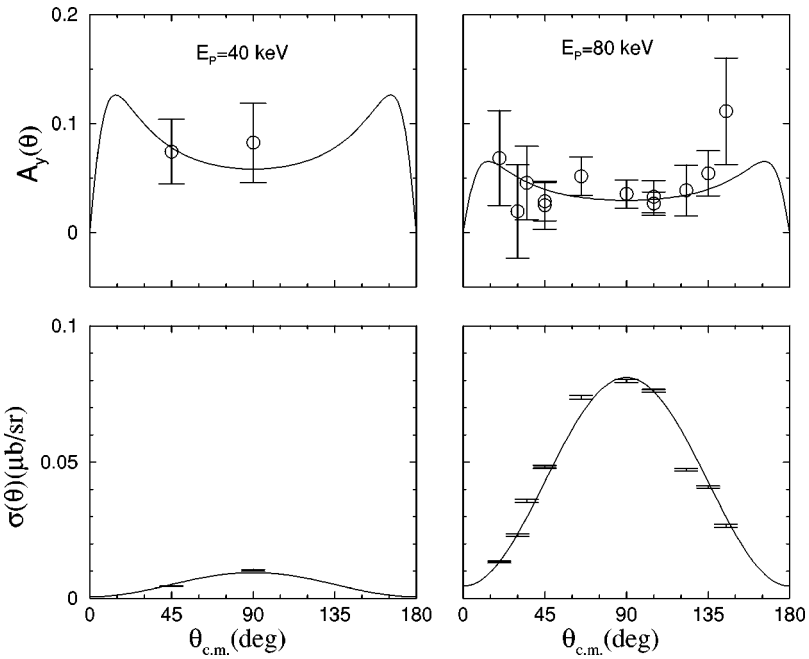

FIG. 2. The angular distributions of the cross section and analyzing power for incident proton energies of 40 and 80 keV. The error bars represent the statistical uncertainties associated with the data points. The solid curves are the result of the TME fit, constrained as described in the text.

present at the energies of our experiment. The *p*-wave capture process can produce a 1^- intermediate state which can then decay via $E1$ radiation to the 0^+ ground state of ^{4}He. Although both $S=0$ and $S=1$ intermediate states are possible, the $S=1(1^-)$ strength would correspond to a spin-flip $E1$ transition and is therefore expected to be very small.

Although the *p*-wave $\Delta S=0$ $E1$ radiation is expected to dominate, we can also expect to observe *s*-wave capture strength, since there is no angular momentum barrier in this case. The *s*-wave capture process can produce a 0^+ or a 1^+ intermediate state, with only the latter allowed to γ decay to the ground state, which it would do via an $M1$ transition. We therefore expect the ^{3}H($\vec{p},\gamma$)^{4}He reaction to be dominated by two transition matrix elements (TMEs) in this very-low-energy regime. We shall label these using the notation $^{2S+1}l_J(pL)$, where *l*, *S*, and *J* are the quantum numbers of the continuum state, *p* specifies the mode of radiation, and *L* is the multipolarity. We therefore have the $^1P_1(E1)$ and the $^3S_1$(M1) TMEs, respectively. Since these are complex quantities, we shall let the above terms represent their magnitudes and define their relative phase to be $\delta_{3S\text{-}1P}$.

It is the magnitudes of these TMEs and their relative phase that determine the angular distribution of the cross section and the analyzing power. Expressions for these observables are conveniently written in terms of the coefficients of expansions in terms of Legendre and associated Legendre polynomials. We write (where for pure dipole radiation $k \leqslant 2$)

$$\sigma(\theta)=A_0\left[1+\sum_{k=1}^{2} a_k Q_k P_k(\cos\theta)\right] \tag{1}$$

and

$$A_y(\theta)=\frac{A_0}{\sigma(\theta)}\left[\sum_{k=1}^{2} b_k Q_k P_k^1(\theta)\right]. \tag{2}$$

The coefficients a_k and b_k, which have been normalized by A_0, can be written in terms of the TMEs involved in the reaction, where we will now also include the $S=1$, $E1$ TME ($^3P_1(E1)$) [18]:

$$a_1=-1.837|^3P_1||^3S_1|\cos\delta_{^3S_1\text{-}^3P_1}, \tag{3}$$

$$a_2=-0.75|^1P_1|^2+0.375|^3P_1|^2, \tag{4}$$

$$b_1=-1.3|^1P_1||^3S_1|\sin\delta_{^3S_1\text{-}^1P_1}+0.92|^3P_1||^3S_1|\sin\delta_{^3S_1\text{-}^3P_1}, \tag{5}$$

and

$$b_2=0.53|^1P_1||^3P_1|\sin\delta_{^3P_1\text{-}^1P_1}, \tag{6}$$

with $A_0=0.75[|^1P_1|^2+|^3P_1|^2+|^3S_1|^2]$. Note that the Q_k coefficients in Eqs. (1) and (2) are used to correct for the finite size of the detector [19]. Note also that (and this is why we included this term in these equations) both a_1 and b_2 are identically zero if the spin-flip $E1$ strength ($^3P_1(E1)$) is zero.

Legendre polynomial fits to the data at 80 keV were performed through order $k=2$. The resulting coefficients are displayed in Table I. As seen here, our data indicate that the neglect of the $^3P_1(E1)$ is a reasonable approximation.

TABLE I. The Legendre and associated Legendre polynomial coefficients obtained from the unconstrained fits to the data at 80 keV.

Coefficient	Value
a_1	0.003 ± 0.002
a_2	1.045 ± 0.002
b_1	0.056 ± 0.021
b_2	-0.001 ± 0.010

TABLE II. The results of the TME analysis using the Coulomb phase shift values given in the text.

TME	% of σ at $E_p=40$ keV	% of σ at $E_p=80$ keV
$^3S_1(M1)$	$(0.44\pm0.28)\%$	$(0.2\pm0.06)\%$
$^1P_1(E1)$	$(99.56\pm0.47)\%$	$(99.8\pm0.71)\%$

The next step in the analysis was to search on the magnitudes and the relative phase of the two TMEs in order to determine the $M1$ strength. However, since the quantity which determines this is essentially only the b_1 coefficient, it can be seen [Eq. (5)] that there is a large ambiguity since the strength and relative phase can be played against one another. In order to obtain a definite result, an additional constraint is required.

Fortunately, our previous studies [1,2] of the *p-d* capture reaction at similar energies showed that the relative *s-p* phase is determined almost entirely by the Coulomb potential. In that case enough observables were measured that a fit without constraints was possible (we also measured tensor analyzing powers using the inverse *d-p* capture reaction). Indeed, the relative *s-p* phase determined by this fitting procedure was found to be equal to the point-charge Coulomb phase difference to within $\pm 6\%$. This was also substantiated by the ''exact'' three-body calculations [7], which showed that the nuclear phase shifts at these energies were only a few tenths of a degree. We therefore fixed the relative phase in Eq. (5) to the point-charge Coulomb phase shift value. The actual value used in the fit was obtained by integrating the Coulomb phase shift over energy—from the initial beam energy to zero, weighted by the yield at each energy. The resulting values were $\delta_{^3S_1\text{-}^1P_1}=-51°$ at $E_p=40$ keV, and $-38°$ at $E_p=80$ keV [20]. The results of a fit to the data of Fig. 2 when the relative phases were constrained to these values produced the solid curves shown in Fig. 2, with the results presented in Table II below.

An alternative to this fitting procedure is to use the value of the b_1 coefficient and solve Eq. (5) along with the normalization relationship $0.75[|^1P_1|^2+|^3S_1|^2]=1.0$ in order to obtain the $^3S_1$ $(M1)$ strength. Keeping only the first term of Eq. (5) and setting the relative phase equal to $-38°$ gives a quadratic equation with two solutions. The value of b_1 used here was, for consistency, obtained from a Legendre polynomial fit where a_1 and b_2 were set equal to zero. The value of b_1 was found to be $b_1=0.053\pm0.021$. Solving the quadratic equation gives a value for the $^3S_1$ $(M1)$ strength of 0.22%, in agreement with the result of the fit given in Table II. The second solution just reverses the $E1$ and $M1$ strengths, but is unacceptable since predominant *s*-wave capture $M1$ strength would lead to a nearly isotropic angular distribution for the cross section in contrast to the data. We can also see that the error in the $^3S_1$ strength ($\sim 30\%$) reflects the percentage error in the b_1 coefficient. It is this sensitivity of the analyzing power which makes it possible to determine the $M1$ strength reported here even though it only accounts for 0.2% of the total cross section to an accuracy of $\pm 0.06\%$.

Recall that these results are for the condition in which both the 40 and 80 keV beams were stopped in the tritiated titanium target. In order to determine the cross section at specific energies and to better understand the implications of the results in Table II, the observed yields were written as an integral over the beam energy in the target (E_p), from the incident energy E_b to zero:

$$Y(E_b)=\epsilon n_p N_t \int \int_{E_b}^{0} \frac{d\sigma(E_p,\theta)}{d\Omega}\frac{1}{\mathrm{STP}(E_p)}dE_p d\Omega, \quad (7)$$

where ϵ is the detector efficiency, n_p is the number of protons which strike the target, and N_t is the atomic number density (by volume) of tritium in the target. The evaluation of this integral requires a knowledge of the stopping powers $[\mathrm{STP}(E_p)]$ for protons in titanium (tritium effects being negligible) as a function of energy, as well as the energy dependence of the cross section $\sigma(E)$. The stopping powers were obtained from [14]. The energy dependence of the cross section, dominated by the Coulomb barrier effects, was expressed using the astrophysical S factor [21]:

$$\sigma(E_{\mathrm{c.m.}})=\frac{S(E_{\mathrm{c.m.}})e^{-2\pi\eta}}{E_{\mathrm{c.m.}}}, \quad (8)$$

where

$$\eta=\frac{1}{2\pi}(31.29)z_1 z_2\sqrt{\frac{\mu}{E_{\mathrm{c.m.}}}}, \quad (9)$$

with μ, the reduced mass in amu, and $E_{\mathrm{c.m.}}$ in keV. Previous studies [22] have shown that the S factor in this energy region (i.e., below 100 keV) is, to a good approximation, a quadratic function of the center-of-mass energy. We therefore write

$$S(E_{\mathrm{c.m.}})=S_0+S_1\times E_{\mathrm{c.m.}}+S_2\times E_{\mathrm{c.m.}}^2. \quad (10)$$

This relationship, when substituted into Eqs. (8) and (7), provides a relationship between the observed yields and the constants of the parametrized S factor as shown in Eq. (10). In order to find these constants, additional data were needed and were obtained from [22,23] in the form of S factor values. A search of the parameters S_0, S_1, and S_2 was then performed which simultaneously fitted our measured yields at $E_b=40$ and 80 keV [calculated using Eqs. (7), (8), and (10)] and these S-factor values [calculated using Eq. (10)] at energies below $E_{\mathrm{c.m.}}=250$ keV. The results are shown in Fig. 3, where the S-factor values corresponding to our two measured yields are plotted at the ''average'' beam energies associated with our incident energies of 40 and 80 keV, respectively—for presentation purposes. The ''average energy'' was taken to be the degraded energy above which one-half of the observed yield originates. The dead layer on the surface of the target, previously described, played a significant role in the values of these average energies, which were determined to be 12.3 and 31.2 keV, respectively. Obtaining a value for the absolute cross section (or, equivalently, the value of S_0) required additional information in-

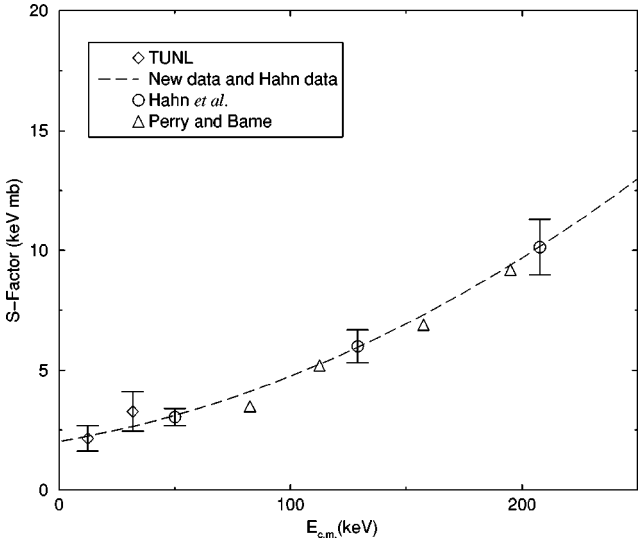

FIG. 3. *S*-factor data of the present (diamonds) and previous [22] works (circles) are shown as a function of center-of-mass proton energy. The dashed curve is a result of a fit to these data, as described in the text. The present data are represented by the two data points plotted at yield-weighted average energies, but were actually yields obtained by stopping the beam in the target, as explained in the text. Data of Perry and Bame [23] (triangles) are also shown.

cluding the detector solid angle and efficiency, the total incident flux, and the tritium areal density in the target. The latter was determined by using the ^{3}H(d,n)^{4}He reaction, as previously discussed. The resulting values for the *S*-factor parameters are

$$S_0=(2.0\pm0.2) \quad \text{keV mb},$$

$$S_1=(1.6\pm0.4)\times10^{-2} \quad \text{mb},$$

and

$$S_2=(1.1\pm0.3)\times10^{-4} \quad \text{mb/keV}.$$

These results are in good agreement with those obtained from a fit to the three points shown from the data of Ref. [22] alone [$S_0=(1.8\pm1.5)$ keV mb, $S_1=(2.0\pm3.4)\times10^{-2}$ mb, and $S_2=(1.1\pm1.4)\times10^{-4}$ mb/keV], indicating that the present results are consistent with those of Ref. [22]. These parameters can be inserted into Eqs. (8) and (10) in order to compute the *S* factor and the absolute cross section of the ^{3}H(p,γ)^{4}He reaction at energies below $E_{\text{c.m.}}=100$ keV where data have not been reported prior to this work. Equation (1) and our previously determined Legendre polynomial coefficients (Table I) can be used to determine the cross section at $\theta=90°$. The results of this calculation are presented in Table III.

Just as the *S* factors were presented at the ''average'' energies for our two measured values at the incident beam energies of 40 and 80 keV, we plot the corresponding cross sections in a similar manner in Fig. 4. The previous cross-section results of [22] are also shown in Fig. 4. An $E1$ direct capture calculation [24] was performed to compare to these

TABLE III. The *S* factor and the integrated and 90° cross sections below $E_{\text{c.m.}}=100$ keV as a function of energy, obtained from Eq. (10) and the adopted values of the *S* factor constants.

$E_{\text{c.m.}}$ (keV)	*S* factor (keV mb)	σ_T (μb)	σ(90°) (μb/sr)
10.0	2.17	0.04	0.005
20.0	2.36	0.27	0.032
30.0	2.58	0.60	0.072
40.0	2.82	0.96	0.114
50.0	3.08	1.32	0.157
60.0	3.36	1.67	0.200
70.0	3.66	2.03	0.242
80.0	3.99	2.39	0.285
90.0	4.34	2.74	0.328
100.0	4.71	3.11	0.371

results. The Woods-Saxon potential used to describe the bound state was adjusted to reproduce the experimental binding energy. And a real potential was used to describe the scattering state. The parameters were adjusted to give the best possible fit to the data of Fig. 4 and are summarized in Table IV. The results of the calculation are shown as the solid curves in Fig. 4. As can be seen in the inset of Fig. 4, this simple model calculation does an excellent job of describing the very-low-energy cross sections of this reaction and agrees with the present and the previous experimental data at these very low energies.

The $M1$ strength observed in the ^{3}H($\vec{p},\gamma$)^{4}He reaction below $E_p=80$ keV can be presented in the form of the $M1$ part of the astrophysical *S* factor. The fact that this strength arises from *s*-wave capture leads, in a direct capture model,

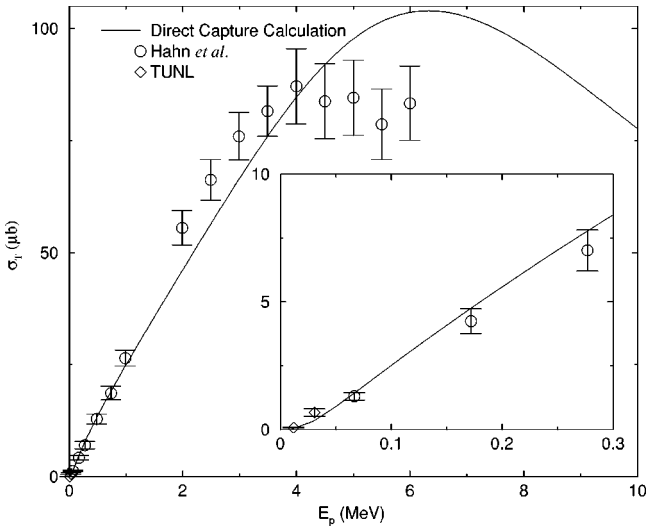

FIG. 4. The cross section for the ^{3}H(p,γ)^{4}He reaction as a function of incident proton energy. The diamonds represent the cross sections of the present work and are plotted at the yield-weighted average energies corresponding to beam energies of $E_p=40$ and 80 keV. Higher-energy data are from [22]. The solid curves (including the one in the inset, which is a blowup of the low-energy region) are the results of an $E1$-only direct capture calculation.

TABLE IV. The Woods-Saxon potential parameters used in the direct capture calculation shown in Fig. 4.

Parameter	Scattering potential (real)	Bound state potential
r_o	1.4 fm	0.96 fm
a	0.65 fm	0.66 fm
r_c	1.2 fm	1.2 fm
V	70 MeV	63 MeV

to a constant value (as a function of energy) for this part of the S factor. An identical behavior for the s-wave $M1$ part of the S factor has been verified by direct measurement in the case of $p+d$ capture [1]. The $M1$ portion of the S factor is therefore a part of S_0 and will be labeled S_s. The remainder of S_0 is attributed to p-wave $E1$ capture, and we write $S_0 = S_s + S_p$. The value we find, based on the percentages given in Table II and the S-factor values given above, is $S_s = 0.008 \pm 0.003$ keV mb.

The cross section for the $^3\mathrm{He}(n,\gamma)^4\mathrm{He}$ reaction has been measured at thermal energies and determined to be $\sigma_{th} = 54 \pm 6$ μb [25,26]. This cross section is interpreted as being purely s-wave $M1$ capture. As a result of the fact that the ground state of ^{4}He is an eigenfunction of the one-body $M1$ operator, it is expected that this $M1$ strength will have a large component which is due to two-body currents, i.e., MEC effects [6]. Indeed, a theoretical analysis has concluded that this strength is almost entirely due to MEC effects (see, however, Ref. [26] and references therein). The $M1$ strength observed in the present study of the $^3\mathrm{H}(\vec{p},\gamma)^4\mathrm{He}$ reaction should be related to this strength. To first order, we would expect the $M1$ cross section in the $^3\mathrm{H}(\vec{p},\gamma)^4\mathrm{He}$ reaction to be equal to that of the $^3\mathrm{He}(n,\gamma)^4\mathrm{He}$ reaction, reduced by the effects of the Coulomb barrier.

A somewhat similar situation occurs in the well-studied case of the three-body system. In that case about 50% of the (s-wave $M1$) cross section of the n-d capture reaction at thermal energies has been shown to be due to MEC effects [3]. A recent determination of the $M1$ cross section in the case of p-d capture below $E_p = 80$ keV has been theoretically analyzed and shown to have a 50% component arising from MEC effects [7]. The relationship between this cross section and the n-d capture cross section is, as in the four-body case above, expected to be determined predominantly by the effects of the Coulomb barrier. In both cases p-d/n-d and p-T/n-^{3}He, the Coulomb barrier between the incoming proton and the proton in the target is expected to reduce the cross section considerably with respect to the neutron capture reaction. Since both of the cross sections are known in the p-d/n-d case, we can use their ratio and compare it to that observed in the present case.

As a result of the rapidly changing value of the cross section of proton capture reactions as a function of energy in this energy regime, it is difficult to compare cross sections of various reactions. However, S_s is a constant which specifies the $M1$ S factor in both the p-d and the p-T capture reactions below 80 keV. In the case of n-d and n-^{3}He, we have experimental values for the thermal neutron capture cross sections. If we assume this ratio is similar for both cases, we can use the ratio of S_s to σ_{th} in the three-body case, along with the measured value of σ_{th} for the n-^{3}He reaction to determine the value of S_s for the present reaction. We find

$$S_s[^3\mathrm{H}(p,\gamma)^4\mathrm{He}] = \frac{S_s[d(p,\gamma)^3\mathrm{He}]}{\sigma_{th}[d(n,\gamma)^3\mathrm{H}]} \times \sigma_{th}[^3\mathrm{He}(n,\gamma)^4\mathrm{He}]$$

$$= \frac{0.055}{254} \times 54 \ \text{keV mb}$$

$$= 0.012 \pm 0.003 \ \text{keV mb},$$

which is in reasonably good agreement with the present experimental result (0.008 ± 0.003 keV mb).

Besides lending credibility to the experimental value of S_s determined in the present work, the above agreement also implies that our value for the overall cross section of the $^3\mathrm{H}(p,\gamma)^4\mathrm{He}$ reaction is correct, at least to within the uncertainty on the value of S_s, which is $\pm 40\%$. Furthermore, the $M1$ strength observed in the present work is most likely due primarily to MEC effects, since it is consistent with the ''Coulomb-corrected'' value of the $M1$ strength observed in the case of thermal neutron capture on ^{3}He.

IV. CONCLUSIONS

This study of the $^3\mathrm{H}(\vec{p},\gamma)^4\mathrm{He}$ reaction at very low energies has provided reliable values of the cross section for this reaction at and below $E_p = 80$ keV. These results should be of practical value in future designs of γ-ray generators which employ this reaction [27]. The present study also determined the value of the astrophysical S factor for the $^3\mathrm{H}(p,\gamma)^4\mathrm{He}$ reaction at $E = 0$ and its slope in the region below 80 keV. The results are in agreement with the previously determined values, which lends credibility to both the previous and present experimental results. Finally, the polarized beam measurements made it possible to extract the $M1$ strength present in the cross section at these low energies, despite its rather small percent contribution to the cross section. The extracted $M1$ strength appears to be consistent with the expected value based on the appropriate (n,γ) to (p,γ) ratio in the three-body system and the thermal neutron capture cross section for ^{3}He. This result makes it very tempting to conclude that, as in the case of thermal neutron capture on ^{3}He, the $M1$ cross section in the $^3\mathrm{H}(p,\gamma)^4\mathrm{He}$ reaction below 80 keV is primarily due to MEC effects. Finally, the $^3\mathrm{He}(p,e^+\nu_e)$ reaction is a likely source of high-energy neutrinos in the Sun, where the average proton kinetic energy is on the order of 1 keV. The cross section for this reaction has been estimated from the measured value of the $^3\mathrm{He}(n,\gamma)^4\mathrm{He}$ reaction at thermal energies using the close relationship between the matrix elements of these two reactions and model calculations [26]. Since the value of S_s for the $^3\mathrm{H}(p,\gamma)^4\mathrm{He}$ reaction determined in the present work is closely related to the $^3\mathrm{He}(n,\gamma)^4\mathrm{He}$ cross section at thermal energies, this result should provide additional tests of the model assumptions and should lead to a more accurate value

of the high-energy neutrino flux expected from the ^{3}He+p reaction in the sun.

Clearly, a firm conclusion and interpretation of our experimental results must await a rigorous four-body calculation which explicitly includes the effects of two-body currents.

ACKNOWLEDGMENTS

This work was partially supported by the U.S. DOE under Contract Nos. DE-FG02-97ER41033, DE-FG02-97ER41047, and DE-FG02-97ER41042.

[1] G.J. Schmid *et al.*, Phys. Rev. Lett. **76**, 3088 (1996); G.J. Schmid *et al.*, Phys. Rev. C **56**, 2565 (1997).
[2] E.A. Wulf *et al.*, Phys. Rev. C **61**, 021601(R) (1999); E. A. Wulf, Ph.D. thesis, Duke University, 1999.
[3] J.L. Friar, B.F. Gibson, and G.L. Payne, Phys. Lett. B **251**, 11 (1990).
[4] L.I. Schiff, Phys. Rev. **52**, 242 (1937).
[5] M. Verdi, Helv. Phys. Acta **23**, 453 (1950).
[6] J. Carlson, D. Riska, and R. Schiavilla, Phys. Rev. C **42**, 830 (1990).
[7] M. Viviani, R. Schiavilla, and A. Kievsky, Phys. Rev. C **54**, 534 (1996).
[8] M. Viviani (private communication).
[9] A. Fonseca (private communication).
[10] T.B. Clegg, Rev. Sci. Instrum. **61**, 385 (1990).
[11] A.J. Mendez, C.D. Roper, J.D. Dunham, and T.B. Clegg, Rev. Sci. Instrum. **67**, 3073 (1996).
[12] Safety Light Corporation, Bloomsburg, PA, 1990.
[13] N. Jarmie, R.E. Brown, and R.A. Hardekopf, Phys. Rev. C **29**, 2031 (1984); **33**, 385 (1986).
[14] H.H. Anderson and J.F. Ziegler, *Hydrogen Stopping Powers and Ranges in all Elements* (Pergamon, New York, 1977).
[15] A. Krauss *et al.*, Nucl. Phys. **A465**, 150 (1987).
[16] H.R. Weller and N.R. Roberson, IEEE Trans. Nucl. Sci. **NS-28**, 1268 (1981).
[17] M.J. Balbes, G. Feldman, L.H. Kramer, H.R. Weller, and D.R. Tilley, Phys. Rev. C **43**, 343 (1991).
[18] R.G. Seyler and H.R. Weller, Phys. Rev. C **20**, 453 (1979).
[19] M.E. Rose, Phys. Rev. **91**, 610 (1953).
[20] I.E. McCarthy, *Introduction to Nuclear Theory* (Wiley, New York, 1968).
[21] C.E. Rolfs and W.S. Rodney, *Cauldrons in the Cosmos* (University of Chicago Press, Chicago, 1988).
[22] K.I. Hahn, C.R. Brune, and R.W. Kavanagh, Phys. Rev. C **51**, 1624 (1995).
[23] J.E. Perry and S.J. Bame, Jr., Phys. Rev. **99**, 1368 (1955).
[24] C. Rolfs, Nucl. Phys. **A217**, 29 (1973).
[25] F.L.H. Wolfs *et al.*, Phys. Rev. Lett. **63**, 2721 (1989).
[26] R. Wervelman *et al.*, Nucl. Phys. **A526**, 265 (1991).
[27] A.W.P. Poon, Ph.D. thesis, The University of British Columbia, 1991.